International Journal for Parasitology: Drugs and Drug Resistance 26 (2024) 100557

Contents lists available at ScienceDirect

International Journal for Parasitology: Drugs and Drug Resistance

journal homepage: www.elsevier.com/locate/ijpddr

A multiplexed high throughput screening assay using flow cytometry identifies glycolytic molecular probes in bloodstream form *Trypanosoma brucei*

Daniel H. Call [a], John Asafo Adjei [a], Ryan Pilgrim [a], James W. Jeong [a], E. Vance Willis [a], Ronald A. Zegarra [a], Nicholas L. Tapia [a], Madalyn Osterhaus [a], Jacob A. Vance [a], Charles M. Voyton [a,b], James A. Call [a], Sabrina S. Pizarro [b,c], James C. Morris [b,c], Kenneth A. Christensen [a,*]

[a] Chemistry and Biochemistry Department, Brigham Young University, Provo, UT, USA
[b] Department of Genetics and Biochemistry, Clemson University, Clemson, SC, USA
[c] Eukaryotic Pathogens Innovation Center, Clemson University, Clemson, SC, USA

ARTICLE INFO

Keywords:
Flow cytometry
High-throughput screen
Biosensor
Glycolysis
Trypanosoma brucei
Metabolism

ABSTRACT

Kinetoplastid organisms, including *Trypanosoma brucei*, are a significant health burden in many tropical and semitropical countries. Much of their metabolism is poorly understood. To better study kinetoplastid metabolism, chemical probes that inhibit kinetoplastid enzymes are needed. To discover chemical probes, we have developed a high-throughput flow cytometry screening assay that simultaneously measures multiple glycolysis-relevant metabolites in live *T. brucei* bloodstream form parasites. We transfected parasites with biosensors that measure glucose, ATP, or glycosomal pH. The glucose and ATP sensors were FRET biosensors, while the pH sensor was a GFP-based biosensor. The pH sensor exhibited a different fluorescent profile from the FRET sensors, allowing us to simultaneously measure pH and either glucose or ATP. Cell viability was measured in tandem with the biosensors using thiazole red. We pooled sensor cell lines, loaded them onto plates containing a compound library, and then analyzed them by flow cytometry. The library was analyzed twice, once with the pooled pH and glucose sensor cell lines and once with the pH and ATP sensor cell lines. Multiplexing sensors provided some internal validation of active compounds and gave potential clues for each compound's target(s). We demonstrated this using the glycolytic inhibitor 2-deoxyglucose and the alternative oxidase inhibitor salicylhydroxamic acid. Individual biosensor-based assays exhibited a Z′-factor value acceptable for high-throughput screening, including when multiplexed. We tested assay performance in a pilot screen of 14,976 compounds from the Life Chemicals Compound Library. We obtained hit rates from 0.2 to 0.4% depending on the biosensor, with many compounds impacting multiple sensors. We rescreened 44 hits, and 28 (64%) showed repeatable activity for one or more sensors. One compound exhibited EC_{50} values in the low micromolar range against two sensors. We expect this method will enable the discovery of glycolytic chemical probes to improve metabolic studies in kinetoplastid parasites.

1. Introduction

Kinetoplastid diseases, including leishmaniasis, Chagas disease, and human African trypanosomiasis (HAT), pose a significant health burden in third-world tropical and semitropical countries (World Health Organization, 2015; Molyneux et al., 2017; World Health Organization, Department of Control of Neglected Tropical Diseases, 2017). While there have been recent advances in therapeutics treating HAT (Mesu

* Corresponding author.
E-mail addresses: kf7jxb@byu.edu (D.H. Call), adjei0@student.byu.edu (J.A. Adjei), ryanpil@student.byu.edu (R. Pilgrim), wookie99@student.byu.edu (J.W. Jeong), vancerwillis@gmail.com (E.V. Willis), ronald2706@hotmail.com (R.A. Zegarra), ctapia1@byu.edu (N.L. Tapia), mosterha@student.byu.edu (M. Osterhaus), jacobav96@gmail.com (J.A. Vance), chuckvoyton570@gmail.com (C.M. Voyton), jamescall2012@gmail.com (J.A. Call), ssutto3@clemson.edu (S.S. Pizarro), jmorri2@clemson.edu (J.C. Morris), ken.christensen@byu.edu (K.A. Christensen).

https://doi.org/10.1016/j.ijpddr.2024.100557
Received 4 April 2024; Received in revised form 17 July 2024; Accepted 1 August 2024
Available online 8 August 2024

et al., 2018), *T. brucei* still has a considerable impact on agriculturally-valuable animals (Eshetu and Begejo, 2015). Additionally, the therapies for the treatment of infections caused by the related parasites *T. cruzi* and *Leishmania species* are not optimal, with drug resistance, adverse side effects, and expense noted as barriers to successful use (Gaspar et al., 2015; Hefnawy et al., 2017; Ponte-Sucre et al., 2017).

Kinetoplastid parasites localize most glycolytic enzymes into specialized peroxisomes called glycosomes (Opperdoes and Borst, 1977; Michels et al., 2021). This compartmentalization distinguishes the kinetoplastid biology from that of their mammalian hosts, making glycolysis and glycosomes potential targets to treat these diseases (Clarkson and Brohn, 1976; Chambers et al., 2008; Coley et al., 2011). However, much remains poorly understood about glycolysis and the glycosome, such as how the resident enzymes are regulated (Dodson et al., 2011; Lin et al., 2017) and how glycolysis and the glycosome participate in regulating cell differentiation (Szöőr et al., 2010; Qiu et al., 2018).

Chemical probes that inhibit enzymes are useful tools for dissecting the roles of those proteins in their metabolic pathways. However, there are few chemical probes available that inhibit specific enzymes in relevant pathways (St. Onge et al., 2012). Discovering novel chemical probes, their target(s), and eventually their modes of action (MOAs) can improve our ability to study the metabolism of these parasites and other eukaryotes. We expect this will lead to better drug targets and therapeutics to treat kinetoplastid diseases.

The traditional method to identify inhibitors with a known MOA is to screen compounds against a purified protein, known as a targeted screen (Sharlow et al., 2010; Swinney, 2013). While this approach can identify potent inhibitors of a known target protein, in vitro compound activity does not necessarily translate to activity in live cells (Gilbert, 2013; Roster et al., 2023). This can result from many factors, such as poor membrane permeability and compound metabolism. The target must also be known in advance, preventing the discovery of novel MOAs (Swinney, 2013). To overcome these setbacks, many scientists have turned to phenotypic screening methods.

In phenotypic screening, compounds are screened against live organisms for a desired phenotype, such as loss of viability. This strategy often identifies novel MOAs of compounds that are effective in live cells (Bowling et al., 2012; Gilbert, 2013; Swinney, 2013). An important drawback of phenotypic screens is that the target(s) and MOAs of hit compounds are generally poorly understood and can be challenging to resolve (Pasquer et al., 2020). This problem can prevent the use of these compounds as chemical probes or therapeutics and hampers efforts to improve their selectivity over human orthologs (Katsuno et al., 2015).

To overcome this setback, we established a phenotypic screen that could also guide target identification and provide clues about MOAs of hit compounds. We developed an assay that can measure multiple metabolic analytes simultaneously (multiplexing) using flow cytometry. Multiplexing can also enable internal validation of hit compounds. Flow cytometry has only recently begun to be widely used for screening due to improvements in throughput (Janzen, 2014). Other laboratories have developed multiplexed screening assays where different cell lines were barcoded with chemical dye(s) to distinguish them when pooled together (Krutzik and Nolan, 2006; Doucette et al., 2016; Ding et al., 2018; Wu et al., 2019; Spurgeon and Naseem, 2020). However, according to our knowledge, no one has used multiplexed screens to explore potential target(s) of hit compounds. In our assay, we screened for glycolytic inhibitors by measuring glycolysis-related analytes in live bloodstream form (BF) *T. brucei* using fluorescent biosensors for glucose, ATP, and glycosomal pH (pH_G), and the cell-impermeable DNA-binding dye thiazole red (TR) to measure cell viability. The synergistic information gained from measuring multiple analytes simultaneously allowed us to identify glycolytic inhibitors and distinguish inhibitors of certain parts of glycolysis. For example, inhibitors of glucose import were predicted to cause a decrease in intracellular glucose, ATP, and possibly pH_G. Inhibitors of downstream glycolysis would decrease ATP, possibly pH_G, but not glucose.

Here, we describe the validation of this high-throughput screening (HTS) assay in a pilot screen of 14,976 compounds from a diverse chemical library. Some of the active compounds identified from the screen were retested to assess reproducibility, potency, and the ability to identify glycolytic inhibitors. We demonstrated this assay can reproducibly identify active compounds for each sensor. Using the sensors together gave synergistic information that cross-validated each active compound and gave clues about their potential target(s). Our findings suggest this method can assist in bridging the gap between phenotypic and target-based drug screening to gain benefits from both screening strategies.

2. Materials and methods

2.1. Cell culture, materials, and reagents

Experiments were performed using *T. brucei* 427 BF or BF 90-13 cell lines. BF cells were continuously cultured in HMI9 media supplemented with 5% fetal bovine serum and 5% Corning Nu-Serum IV. Cell culture media components, including the selection antibiotics (blasticidin, G418, and hygromycin) were purchased from Sigma (St. Louis, MO). Zeocin was purchased from InvivoGen (San Diego, CA). GenClone Dulbecco's PBS (DPBS) was purchased from Genesee Scientific (El Cajon, CA). Thiazole red, known as TO-PRO®-3, was purchased from Biotium (Cat. # 40087, Fremont, CA). Propidium iodide was purchased from Biotium (Cat. # 40016, Fremont, CA). 2-deoxy-D-glucose was purchased from Cayman Chemical (Cat. # 14325, Ann Arbor, MI). Salicylhydroxamic acid was purchased from Sigma-Aldrich (Cat. #S607, St. Louis, MO). Flat-bottom 384-well plates, serial number 781620, were purchased from BrandTech Scientific. A custom acrylic plate stand (length: 127.55 mm, width: 85.05 mm, height: 5.65 mm) was cut in-house to bring the plate height to 14.5 mm. This allowed the CytKick Max Auto Sampler to recognize and run the plate. V-bottom reservoirs (15 mL, 12-well, serial number 360102) were purchased from NEST (Wuxi, Jiangsu, China).

2.2. Cloning and transfection

The biosensor AT1.03^{YEMK} (YEMK) was used to measure ATP (Imamura et al., 2009). We cloned this gene from pDR-GW AT1.03YEMK (Bermejo et al., 2010), which was a gift from Wolf Frommer (Addgene plasmid # 28004; http://n2t.net/addgene:28004; RRID:Addgene_28004) into the *T. brucei* BF expression vector pXS6.Q by PCR (see Supplemental Fig. 1 for the cloning scheme). The forward and reverse primers used to amplify the AT1.03^{YEMK} gene and add on the *Bam*HI and *Hin*dIII restriction digest sites were gatggatccctcgagtatggtgag and attcaagcttactcgatg, respectively. The glucose sensor FLII^{12}Pglu-700μδ6 (FLIP700) was cloned into pXS6 as previously described (Voyton et al., 2018b) while the glycosomal pH sensor pHluorin2-PTS1 (pHL) was cloned into the inducible trypanosome expression vector pLEW100v5 (Addgene plasmid # 213776; http://n2t.net/addgene:213776; RRID:Addgene_213776) through HiFi assembly as previously described (Call et al., 2024). Parasites were transfected and selected as described by Wang et al. (2000).

2.3. BF T. brucei culture

BF cultures were counted by flow cytometry on an Attune NxT flow cytometer using a CytKick Max Auto Sampler. Cultures were diluted daily to ~2.0×10^5 cells/mL to maintain cell densities at ~ 1–2.0×10^6 cells/mL for use the following day. Parasites expressing biosensors in pXS6.Q were grown in media containing G418 (1.5 μg/mL). Parasites expressing biosensors in pLEW100v5 were grown in the presence of G418 (1.5 μg/mL), hygromycin (5 μg/mL), and zeocin (2.5 μg/mL). To

induce biosensor expression in parasites harboring pLEW100v5_pHluorin2-PTS1, doxycycline (1 μg/mL) was added. To maintain high expression, experiments were only performed using cells induced for one day to express the transgene. 427 WT cells were grown in media without antibiotics.

2.4. Determining the optimal thiazole red concentration to measure cell viability

Cells were stained with thiazole red (TR) to distinguish dead cells from live cells, based on a flow cytometry method performed on malaria parasites (Russo et al., 2009). To determine the optimal concentration of TR for our HTS assay, BF WT parasites were fixed with 1.3% paraformaldehyde in DPBS (15 min, RT) (Tetaud et al., 2001; Höög et al., 2010) and stained with varying concentrations of TR. The samples were then measured by flow cytometry (637 nm excitation, 670/14 nm emission). Fixed samples were compared to unfixed samples to determine the impact of fixing on cell morphology as measured by FSC-A and SSC-A.

2.5. Validation of biosensor cell line localization and multiplexing

To validate multiplexing of pHL with YEMK or FLIP700, each cell line (WT, pHL, FLIP700, and YEMK) was grown to 1-2 x 10^6 cells/mL as described above. Cells (5 mL) were centrifuged (1000×*g*, 10 min, RT), resuspended in DPBS (1 mL), and aliquots were removed to use as single cell-line controls. The remainder of each sample was used to make two pooled samples: a FLIP700 and pHL duplex and a YEMK-pHL duplex. The samples were centrifuged for 5 min and resuspended in DPBS supplemented with 5 mM glucose, 0.1% DMSO, and 100 nM TR. The samples were incubated on a shaker (37 °C, 10 min) protected from light then incubated (1.5 h, RT) with shaking. After incubation, the samples were analyzed on the Attune NxT flow cytometer using the settings described in the HTS Assay section. Data was analyzed on FCS-Express using the outline described in the HTS Data Analysis section.

Cells were imaged on an ImageStream Mk II flow cytometer (CYTEK, Fremont, CA) to confirm sensor subcellular localization. The lasers used were 405 nm (120 mW), 488 nm (100 mW), and SSC (1.72 mW). Cells were measured at 60× magnification at low speed. We recorded 500 to 1000 cells of each biosensor cell line. We analyzed the data using IDEAS software. In focus cells were gated using Gradient RMS in the brightfield channel. Singlets were gated using Area from and Aspect Ratio from the brightfield channel. To gate for fluorescent cells, we used the intensity of channel 1 (emission 457/45) and channel 2 (emission 533/55). Representative images were chosen for each biosensor cell line.

2.6. Validating multiplex assays with known glycolytic inhibitors

To validate the assay using known inhibitors of glycolysis, cells were washed twice in DPBS, then resuspended in DPBS with no glucose (low control) or DPBS supplemented with 5 mM glucose (high control) and incubated (37 °C, 10 min). An aliquot of the 'high control' was treated with 2-deoxy-d-glucose (2-DG, 50 mM). TR (100 nM) in DMSO (0.01%) was then added to all samples, followed by incubation (90 min, RT, gently shaking, protected from light). The samples were then analyzed by flow cytometry. To obtain biological replicates, the experiment was repeated three separate times. One-way ANOVA was performed to determine if the 2-DG treatment was statistically different from the high and low controls.

A similar assay was conducted for the salicylhydroxamic acid (SHAM) and glycerol experiments; however, additional controls were required. Cells were resuspended in DPBS with 0.11% DMSO; a portion was set aside to use as the 'low control' and the remainder supplemented with 5 mM glucose (high control), followed by incubation (37 °C, 10 min). Samples supplemented with glucose were then treated with SHAM (300 μM), glycerol (5 mM), or a combination of the two, followed by incubation (RT, 90 min, gently shaking, protected from light).

A similar assay was performed to demonstrate that this multiplex screening method could identify inhibitors of glucose transport or pyruvate/proton transport. Important details of these assays are as follows: each duplex (FLIP700-pHL and YEMK-pHL) was incubated in DPBS supplemented with 100 nM TR in DMSO (0.11%) with or without 5 mM glucose. A separate sample was prepared with 5 mM glucose and 100 μM phloretin (a glucose transport inhibitor) or 12.5 mM pyruvate (a pyruvate/proton transport inhibitor). All samples were incubated (RT, 90 min, gently shaking, protected from light). The samples were then analyzed by flow cytometry. One-way ANOVA was performed as previously described.

2.7. Z′-factor assays

The Z′-factor statistics for the assays were resolved to quantify the robustness of the approach (Zhang et al., 1999). To evaluate the suitability of each biosensor for HTS, we measured the Z′-Factor for each biosensor cell line individually and pooled. Cells incubated in 'high' (5 mM glucose, 0.1% DMSO) and 'low' (0 mM glucose, 0.1% DMSO) solution were loaded into half of a 384-well plate and analyzed using an Opentrons2 pipetting robot. To determine the Z′-factor (Zhang et al., 1999), we calculated the average (AVG) and standard deviation (SD) of the ratio of VL2-H (405 ex, 542/27 em) and BL1-H (488 ex, 530/30 em) (VL2/BL1) for the samples after performing slope correction. We then used equation (1) below to calculate the Z′-factor statistic.

$$\text{Z}'\text{-Factor} = 1 - \frac{3\,SD_{High} + 3\,SD_{Low}}{|AVG_{High} - AVG_{Low}|} \quad (1)$$

2.8. Flow rate optimization

To determine the optimal flow rate for running the 384-well plate on the Attune NxT flow cytometer Cytkick autosampler, YEMK-expressing parasites were prepared as described in section 2.7 for the Z′-factor assay. Four flow rates (100, 200, 500, and 1000 μL/min) were tested to determine the highest flow rate achievable without compromising data quality. Three columns of 'high' and 'low' controls on a 384-well plate were tested for each flow rate, and Z′-factors were calculated as described in section 2.3. We compared the Z′-factors for each flow rate to assess the impact of flow rate on data quality. These results guided our decision on the HTS assay's flow rate.

2.9. HTS assay

Each biosensor cell line and WT were grown to 1-3 x 10^6 cells/mL. Each cell line was prepared as described above and resuspended in 1 mL DPBS and a 5 μL aliquot of each was transferred to DPBS to a final volume of 500 μL in separate tubes for single-sensor controls. We then combined the remainder; the pooled sample was centrifuged (5 min, 1000×*g*), and the supernatant was removed. Samples were washed twice before resuspension in 72 mL of DPBS supplemented with 100 nM TR. A 360 μL cell solution aliquot was removed to use as a 'low' control. Glucose was added to 5 mM, and the cell solution was incubated (10 min, 37 °C) with shaking at 250 rpm and then transferred to eight wells of a 12-well reservoir (9 mL per well). The cell solution was aliquoted into two 384-well plates preloaded with test reagent using an Opentrons2 pipetting robot. The final DMSO concentration in each well did not exceed 0.11% based on volume. Plates were covered with a plate seal, wrapped in aluminum foil to protect from light, and incubated (1.5 h, RT, shaking gently). While one plate was analyzed on the flow cytometer, those in cue were stored at 4 °C and protected from light for up to 2 h. Attune settings for the plate run are as follows: high-throughput mode (1 mL/min, 20 μL analyzed/sample, 1 mix/well, no rinses) with boost mode. FSC (H, A, and W), SSC (A), VL2-H (405 ex, 542/27 em), BL1-H (488 ex, 530/30 em), and RL1-H (TR, 637 ex, 670/14 em)

channels were scored. Each plate took approximately 1.5 h to run on the flow cytometer.

2.10. HTS data analysis

FCS data were analyzed in FlowJo_v10.9.0 using templates to achieve consistency and automate the analysis. The samples were divided into three groups to assist downstream analysis: Tube Controls, High Controls, and Samples. Dead cells were distinguished using TR measured on the RL1-H channel. Live and Dead populations were gated using a bisector gate. Cells were gated for using FSC-A vs SSC-A. Doublets were excluded using both FSC-A vs FSC-H. FRET and pHL biosensors were segregated on a dot plot using VL2-H vs BL1-H. Cells with low biosensor fluorescence relative to WT and single-sensor controls were excluded. The following statistics were exported in a CSV file: total count, pHL count, FRET sensor count, percent Live, percent Dead, median fluorescence intensity (MFI) pHL VL2, MFI pHL BL1, MFI FRET sensor VL2, and MFI FRET sensor BL1.

To increase the data analysis throughput and to mitigate errors in analysis, data analysis steps were performed using a Python program called "drugscreen-ph-flip700-yemk-live," found on GitHub. The directions for how to use the program are in the supplementary document Supporting Information 1 - Python Program Instructions. Briefly, the program calculated ratios of the VL2-H and BL1-H median fluorescent intensities (VL2/BL1) for each biosensor. Each well was given a "relative well number" based on the order in which the wells were run. A linear regression model was used to correct the baseline of all samples and controls on each plate to mitigate potential distortions resulting from instrument drift. The correction was carried out using equation (2).

$$y_{corrected} = y_{raw} - m_{raw} \times Relative\ well\ number \quad (2)$$

where m_{raw} is the slope of the slope from the linear regression of VL2/BL1 versus the relative well number, y_{raw} is the original VL2/BL1 ratio, $y_{corrected}$ is the corrected VL2/BL1 ratio, and the *Relative well number* is the number of the sample in the order it was run on the plate. After correcting the slope, compounds with VL2/BL1 ratios exceeding 1.5 standard deviations (SD) *above* the mean were excluded to minimize the influence of fluorescent compounds on the mean and variability of the plate's dataset. Once these outliers were excluded, we calculated a new mean and SD, which we used to convert each biosensor measurement (fluorescence ratio or percent live) into a Z-score (Z_i) using equation (3) (Brideau et al., 2003).

$$Z_i = \frac{y_i - \bar{y}}{SD_y} \quad (3)$$

where y_i is the raw value, $\bar{y}$ is the mean of all wells on the plate (samples and controls), and SD_y is the standard deviation. This allowed the comparison of data across different plates from runs on different days (Brideau et al., 2003). Hits were identified as compounds that yielded results that were at least five SD *below* the mean. Graphs were generated using GraphPad Prism software. The Python program called "analysisConcatinator" (see Supporting Information 3 - Python Program Instructions) was used to concatenate hits together for further analysis. Venn diagrams were created using the tool at https://bioinformatics.psb.ugent.be/webtools/Venn/. The percentage hit rate for each sensor was calculated using equation (4) (Shun et al., 2011).

$$Hit\ Rate = \frac{100 * Number\ of\ Hits}{Total\ Screened\ Compounds} \quad (4)$$

2.11. Optimizing incubation conditions

To increase the assay's throughput, we tested if multiple plates could be prepared in one batch, with later plates incubated at 4 °C while the first plate was analyzed on the flow cytometer. To determine if prolonged incubation at 4 °C impacted data quality, we prepared YEMK-expressing cells as described in section 2.10 for the HTS assay, except that propidium iodide (PI) was used to stain for viability rather than TR. PI was chosen in this experiment since we were not directly using the biosensor measurements. Two 384-well plates were loaded and incubated at room temperature for ~1 h. Then, both plates were incubated at 4 °C, one plate for 1.5 h and the other for 3 h. The 'Percent Live' gate was drawn on the PI-negative population in a histogram using the YL2-H channel (561 ex, 620/15 em) to measure PI fluorescence. 'Percent Live' was plotted versus relative well number to visualize how cell viability changed over time.

2.12. Glucose dose-response multiplex screen validation assay

To explore why many compounds decreased cytosolic glucose but not ATP or pH_G, we incubated each duplex (FLIP700-pHL and YEMK-pHL) in 1:3 serial dilutions of glucose from 50.00 mM to 0.02 mM 100 nM TR and 0.1% DMSO were also present in the buffer. The serial dilutions were prepared at 10X the final concentration in V-bottom 96-well plates. Low control wells were included with no glucose present. After the 1.5-h incubation (RT, shaking gently, protected from light), the plate was analyzed by flow cytometry. Three biological replicates were obtained by repeating the experiment on three separate days. The flow cytometry data was analyzed in FlowJo, and then the exported data for each biosensor was normalized to the highest glucose concentration (50 mM) and the Low control (0 mM glucose). The glucose dose-response EC_{50} for each biosensor was calculated using equation (5) by nonlinear regression (4-parameter model, [agonist] vs response) in GraphPad Prism.

$$Y = Bottom + \frac{\left(X^{HillSlope}\right) * (Top - Bottom)}{X^{HillSlope} + EC50^{HillSlope}} \quad (5)$$

The terms in the equation are as follows: Top is the upper plateau of sensor response, Bottom is the lower plateau of sensor response, Y is normalized sensor response, X is compound concentration, EC50 is potency in μM, and HillSlope is the slope factor.

2.13. Rescreening select hits

To score the reproducibility of hits identified in this HTS, 44 compounds that were hits for one or more sensors were acquired and retested. They were first screened at 10 μM and Compounds that passed the threshold for one or more sensors (<90% live for viability, −50 for ATP, −10 for pH_G, and −10 for glucose) were diluted in a 1:2 serial dilution from 10 μM to ~ 0.08 μM and analyzed in round-bottom 96-well plates. Each threshold was tailored to its sensor as each sensor possessed inherent differences. Low controls (cells in 0 mM glucose and 0.1% DMSO) were included on the plate to enable us to normalize results to controls. EC50 values were determined by fitting the results for each serially diluted compound to the model in equation (6) by nonlinear regression in GraphPad Prism.

$$Y = Bottom + \frac{Top - Bottom}{1 + \left(\frac{EC50}{X}\right)^{HillSlope}} \quad (6)$$

The terms in the equation are as follows: Top is the upper plateau of sensor response, Bottom is the lower plateau of sensor response, Y is normalized sensor response, X is compound concentration, EC50 is potency in μM, and HillSlope is the slope factor.

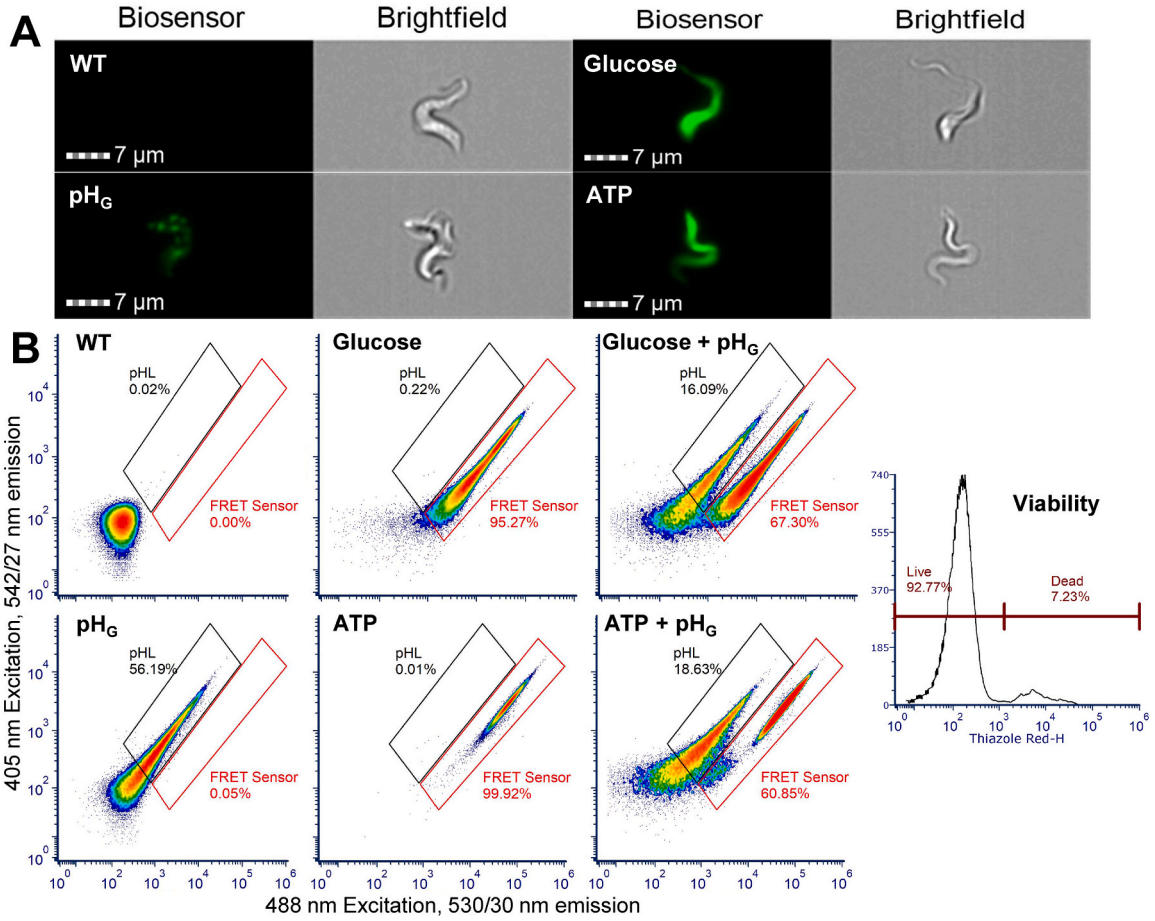

Fig. 1. Engineering biosensor cell lines for the HTS method. A) pHL (glycosomal pH sensor) was localized to the glycosome. FLIP700 (Glucose sensor) and YEMK (ATP sensor) were localized to the cytosol. B) Dot plots of each biosensor cell line compared to WT. pHL could be distinguished from the FRET sensors without an additional barcode. Thiazole red (Viability sensor) was included to screen for compounds impacting viability. (For interpretation of the references to colour in this figure legend, the reader is referred to the Web version of this article.)

3. Results and discussion

3.1. Engineering three biosensor cell lines to screen for glycolytic inhibitors

Our lab had previously performed a high-throughput screen by flow cytometry using a FRET glucose biosensor, FLII^{12}Pglu-700µδ6 (FLIP700) (Voyton et al., 2018a). To develop a multiplex flow cytometry high-throughput screen (HTS) assay, we first engineered several *T. brucei* BF cell lines to express biosensors relevant to glycolysis. As ATP is indicative of glycolytic activity in BF *T. brucei*, we engineered a cell line constitutively expressing the FRET ATP biosensor AT1.03^{YEMK} (YEMK) (Imamura et al., 2009). The sequenced plasmid of the AT1.03^{YEMK} gene in the BF *T. brucei* constitutive expression vector pXS6. Q has been submitted to Addgene.

In *T. brucei*, the first seven steps of glycolysis and glycerol kinase are localized to specialized peroxisomes called glycosomes (Opperdoes and Borst, 1977; Michels et al., 2021). At least two of these enzymes, hexokinase and phosphofructokinase, are pH-sensitive (Nwagwu and Opperdoes, 1982; Dodson et al., 2011), indicating glycosomal pH (pH$_G$) may play an important role in glycolysis regulation. Additionally, pH$_G$ actively changed in response to glucose in procyclic form *T. brucei* (Lin et al., 2017). This suggests that pH$_G$ may also be used as a readout of glycolysis, providing some internal cross-validation. To measure pH$_G$, we developed an inducible cell line expressing a glycosomally localized pH sensor. This pH sensor, pHluorin2 (pHL) (Mahon, 2011), was localized to the glycosome using an AKL C-terminal PTS1 tag, a technique our lab has successfully used with other biosensors (Voyton et al., 2018b). As shown in Fig. 1A, pHL was punctate as expected for glycosomal localization. FLIP700 and YEMK were diffuse as expected for cytosolic localization.

3.2. FRET biosensors can be distinguished from pHL when pooled

Pooling biosensors together in the same sample enables the measurement of multiple analytes in the same compound treatment (Doucette et al., 2016), effectively performing multiple screens simultaneously. Multiplexing also enables all sensor cell lines to experience the same treatment conditions, increasing the validity of correlations between different sensors. However, most biosensors use highly similar fluorescent proteins, making it challenging to distinguish them from each other. A common solution is chemically barcoding separate cell lines (Doucette et al., 2016). We performed an alternative approach by pooling one FRET biosensor (either FLIP700 or YEMK) with the single GFP biosensor pHL, enabling multiplex analysis without an additional barcode.

As shown in Fig. 1B, the FRET biosensors could be distinguished from pHL without a barcode. Additionally, the percentage of cells sufficiently fluorescent to be distinguished from the background was greater than 90% for FLIP700 (glucose sensor) and YEMK (ATP sensor) and greater than 50% for pHL. This indicated that more pHL-expressing cells were needed relative to the FRET biosensor cell lines to ensure that each cell line was sufficiently represented. While other labs have demonstrated barcode multiplexing by flow cytometry (Doucette et al., 2016), these

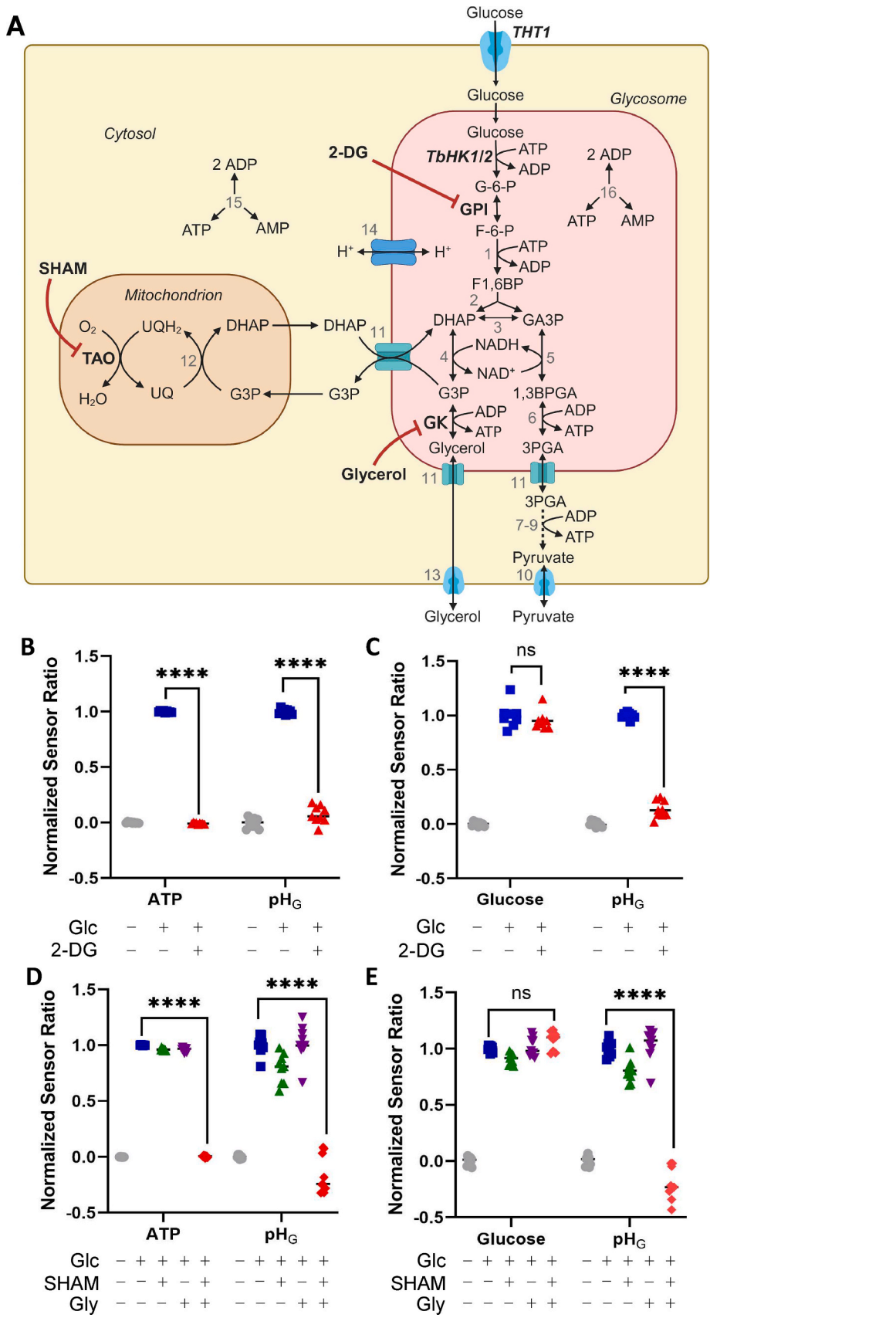

(caption on next page)

Fig. 2. Validating the multiplex HTS method on known glycolytic inhibitors. A) Diagram of glycolysis in BF *T. brucei*. 2-deoxyglucose (2-DG) gets phosphorylated by hexokinase, and the buildup of 2-DG-6-phosphate inhibits glucose-6-phosphate isomerase. SHAM inhibits trypanosome alternative oxidase, and excess glycerol inhibits the forward reaction of glycerol kinase. Solid arrows represent single reactions, while dashed arrows represent multiple reactions. The numbered enzymes are: 1, phosphofructokinase; 2, aldolase; 3, triose phosphate isomerase; 4, glycerol-3-phosphate dehydrogenase; 5, glyceraldehyde-3-phosphate dehydrogenase; 6, phosphoglycerate kinase; 7, phosphoglycerate mutase; 8, enolase; 9, pyruvate kinase; 10, pyruvate transporter TbPT0; 11, unidentified glycosome pore-forming channel(s); 12, glycerol-3-phosphate dehydrogenase; 13, aquaporins TbAQP1-3; 14, unidentified proton transporter; 15, adenylate kinase ADKA, B, C, E, F, and G; 16, ADKD. Abbreviations: THT1, trypanosome hexose transporter 1; TbHK1/2, hexokinase 1 and 2; GPI, glucose-6-phosphate isomerase; TAO, trypanosome alternative oxidase. G-6-P, glucose-6-phosphate; F1,6BP, fructose-1,6-bisphosphate; DHAP, dihydroxyacetone phosphate; GA3P, glyceraldehyde-3-phosphate; G3P, glycerol-3-phosphate; 1,3BPGA, 1,3-bisphosphoglycerate; 3 PG, 3-phosphoglycerate; UQ, ubiquinone; UQH_2, ubiquinol. Created using Biorender.com. B) The ATP and pH_G biosensors were pooled and placed in DPBS in the presence (blue squares) or absence (gray circles) of 5 mM glucose (Glc). A third condition included cells in DPBS with 5 mM glucose and 50 mM 2-DG (red triangles). C) The glucose and pH_G biosensors were pooled and treated in identical conditions as in B. D) The ATP and pH_G biosensors were pooled and placed in DPBS in the presence (blue squares) or absence (gray circles) of 5 mM glucose. Additionally, cells in glucose were treated with either 300 μM SHAM (green upward triangles), 5 mM glycerol (purple downward triangles), or a combination of both (red diamonds). Each treatment was in the presence of 0.1 % DMSO. E) The glucose and pH_G biosensors were pooled and treated in identical conditions as in Fig. 2D. Gly stands for glycerol. **** means p-value <0.0001 by RM one-way ANOVA.(For interpretation of the references to colour in this figure legend, the reader is referred to the Web version of this article.)

results demonstrated FRET and single-GFP biosensors can be distinguished without an additional barcode, enabling a simplified multiplexed analysis of the library. Further, the addition of TR to measure viability was anticipated to not interfere with sensors, as the dye has spectral properties distinct from the biosensors. Staining with TR was optimized (Supplemental Fig. 2), with 100 nM showing the best performance for distinguishing live versus dead cells.

3.3. The multiplex screening method can identify glycolytic inhibitors

One of the advantages of multiplexing different metabolite sensors together is that they can give complementary information, which can narrow down the potential metabolic step that a compound may be inhibiting. Most of the enzymes and transporters involved in *T. brucei* BF glycolysis are known (Fig. 2A), with most validated as therapeutic targets (Wiemer et al., 1995; Uzcategui et al., 2004; Ginger et al., 2005; Chaudhuri et al., 2006; Sanchez, 2013; McNae et al., 2021; Roster et al., 2023). However, there is little known about the intricacies of glycolysis in *T. brucei*, including its regulation (Bakker et al., 1999; Michels et al., 2021) and the identity of glycosome metabolite transporters and pore/channel proteins (Igoillo-Esteve et al., 2011; Gualdron-López et al., 2012; Gualdrón-López et al., 2013). This multiplex screening method aimed to discover chemical probes that perturb glycolysis. These probes could potentially help dissect metabolism and metabolic regulation in trypanosomes and related organisms.

Theoretically, biosensors for glucose, ATP, and pH_G can identify

Table 1
Parameters for Multiplexed biosensor Small Molecule Screen.

Category	Parameters	Description
Assay	Nature of the assay	Cell-based fluorescence flow cytometry assay
	Assay strategy	Simultaneously measure three glycolytic metabolites (ATP or glucose, glycosomal pH, and viability) using endogenously expressed fluorescent biosensors localized to the cytosol or glycosome. FRET sensors are distinguished from GFP-based sensors based on intrinsic differences in fluorescence in measured violet and blue channels.
	Assay protocol	Key steps are presented in Table 2.
Library screened	Nature of the library	Curated library to maximize chemical diversity around common drug criteria
	Size of the library	14,976 compounds from 100,000 compounds arrayed in 384-well plates at 10 mM in DMSO
	Source	Life Chemicals Compound Library LC1 and LC2 from the University of Wisconsin-Madison Small Molecule Screening Facility
	Details	
	Quality control	Hits resynthesized/purchased and verified to be >95% purity
	Concentration tested	10 μM concentration, 0.1% DMSO, 1:100 dilution
HTS process	Format	80 μL 384-well plate (BrandTech 781620)
	Plate controls	Positive control: daily tube of multiplexed cell lines incubated for 1 h in DPBS, 100,000 events collected; Negative control: 5 mM glucose plus 0.1% DMSO in either columns 1–2 or 23–24)
	Plate number and duration	39,384-well plates over 10 days, 4 plates per day
	Reagent and compound dispensing systems	Cells dispensed using Opentrons2 pipetting robot (OT-2)
	Output, detector, analysis software	Channels VL1, VL2, and BL1; analyzed on FlowJo/FCS-Express
	Baseline correction	Perform linear regression to create a trendline. subtract y-intercept from each point in the trendline to find the baseline correction. Baseline-corrected fluorescence ratio = raw ratio - baseline correction
	Normalization	normalized response = (sample result − mean low controls)/(mean high controls − mean low controls)
	Performance	Individual Z'-Factor: YEMK = 0.97, FLIP700 = 0.83, pHL = 0.79 Pooled Z'-Factor: YEMK = 0.93, FLIP700 = 0.95, and pHL = 0.68
Post-HTS analysis	Selection of actives	Active compounds (hits) selected using a threshold five standard deviations below mean value for all compounds and controls baseline on each plate. Sensor values converted to Z-score to enable comparison between plates
	Selection of threshold	5 standard deviations (−5 Z-score) below all samples and controls for each biosensor
	Retesting of initial actives	Complete library screened in duplicate
	Structure confirmation	Structure verified by analytical chemistry methods
	Compound purification/ resynthesis	Hits that repeatably cross the threshold were resynthesized and tested in 8-point dose response
Screen results	List of all screening positives	List of hits for each measured metabolite, as well as list of hits positive for multiple metabolites. Hits ranked by magnitude of metabolite level change
	List of validated compounds	Hits rank ordered based on threshold criteria
	Comments on active compound selection	Metabolite(s) impacted, percentage of impact, and sensor EC_{50} values

Table 2
Multiplexed Biosensor flow cytometry HTS protocol.

Step	Parameter	Value	Description
1	Controls	0.08 μL	DMSO
2	Library compounds	0.08 μL	10 μM
3	Addition of cells	80 μL	Measured 5000–15,000 BF cells per biosensor; 20,000–40,000 total events per well
4	Incubation time	1.5 h	Room temperature
5	Assay readout	405 ex, 542/27 em (VL2); 488 ex, 530/30 em (BL1); 637 ex, 670/14 em (Thiazole Red)	Attune NxT with Cytkick Autosampler flow cytometer

Step	Notes
1	BrandTech 781620 nonsterile 384-well plates atop a custom plate stand. Compound/DMSO was pre-dispensed into each well. DMSO controls in columns 1–2 or 23–24 depending on the plate.
2	Two biosensor BF cell lines (either pHL and YEMK or pHL and FLIP700) and BF WT were washed twice in DPBS then resuspended in DPBS and pooled after the first wash. Aliquots of each biosensor cell-line were taken to use as single-sensor controls after the first wash.
3	The multiplexed cell solution was incubated (10 min, 37 °C, shaking at 250 rpm) to allow cell metabolism to equilibrate. The cell solution was transferred to a reservoir compatible with the Opentrons2 robot, 9 mL/reservoir well.
3	The multiplexed cell solution was pipetted into each well using an Opentrons2 robot; tips were changed between steps.
4	Two plates were loaded with cell solution at a time.
5	Plates were covered with plate seals and incubated at room temperature for 1.5 h.
6	Plates waiting to be run were incubated in the refrigerator at 4 °C in the dark until their turn.
7	Plates were analyzed on an Attune NxT flow cytometer using a CytKick Autosampler; the plate was run using high-throughput mode (1 mL/min flow rate, 20 μL/well analyzed, boost-mode used, 1 mix/well, no washes). One plate took ~1.5 h to finish analysis on the flow cytometer.
8	Measurement settings: VL2, BL1, and Thiazole Red channels were collected for each cell. The VL2/BL1 ratio was taken to measure the relative analyte concentration change for each biosensor.

glycolytic inhibitors in BF *T. brucei* because these three analytes are directly related to glycolysis in this life stage. Glycolysis inhibitors are expected to decrease ATP and pH_G in BF *T. brucei* as glycolysis is the primary pathway through which ATP is generated, and pH_G is associated with ATP (Lin et al., 2017; Michels et al., 2021; Call et al., 2024). Glucose transport inhibitors are expected to decrease at least intracellular glucose. Compounds that only impact pH_G may inhibit proton efflux from the cell, such as the pyruvate-proton symporter (Vanderheyden et al., 2000).

To test whether this multiplex screening assay could identify glycolysis inhibitors, we tested two well-characterized glycolytic inhibitors: 2-deoxyglucose (2-DG) and salicylhydroxamic acid (SHAM). 2-DG competes with glucose for transport into the cell (through THT1/2), is a competitive inhibitor of hexokinase (Gruenberg et al., 1978; Morris et al., 2006; Kovářová et al., 2018), and blocks glycolysis as 2-DG-6-phosphate (Wick et al., 1957; Barban and Schulze, 1961). A high concentration of 2-DG (50 mM) decreased cellular ATP levels even in the presence of glucose (Fig. 2B). This is likely because the accumulation of 2-DG-6-phosphate, which could not be metabolized further, competitively inhibited glucose-6-phosphate isomerase (GPI) which decreased glycolytic flux and subsequent ATP production (Laussel and Léon, 2020).

Interestingly, 2-DG did not significantly decrease intracellular glucose levels (Fig. 2C), likely because glucose was present in the buffer. Since 2-DG is structurally similar to glucose, a logical concern is whether the glucose sensor FLIP700 could distinguish between glucose and 2-DG. We believe FLIP700 did not respond significantly to 2-DG for two reasons. First, FLIPglu-600μ, the predecessor of FLIP700, could discriminate between glucose and 2-DG (Fehr et al., 2003). Second, 2-DG competed with glucose and decreased the measured glucose levels when using FLIP700 in live procyclic form *T. brucei* cells (Voyton et al., 2018a, 2018b). These lines of evidence suggest that 2-DG had a minimal effect on FLIP700 at the concentration tested. However, the sensitivity of FLIP700 to 2-DG has not been directly tested, so we cannot rule out some cross-sensitivity of FLIP700 for 2-DG.

Both procyclic form and BF *T. brucei* acidify their glycosomes when starved for glucose (Lin et al., 2017; Call et al., 2024). Similarly, 2-DG treatment resulted in glycosome acidification (Fig. 2B and C). Notably, 2-DG did not impact cell viability during the 1.5-h incubation (Supplemental Fig. 3).

The combination of SHAM and glycerol perturbs *T. brucei* glycolysis and decreases cellular ATP levels. SHAM inhibits the alternative oxidase, which is necessary for recycling glycerol-3-phosphate to dihydroxyacetone phosphate and the associated removal of excess reducing equivalents (Fig. 2A). Glycerol inhibits a backup pathway where glycerol-3-phosphate is converted to glycerol by glycerol kinase (Clarkson and Brohn, 1976; Clarkson et al., 1981; Helfert et al., 2001; Ebiloma et al., 2019). The combination of SHAM and glycerol significantly decreased cellular ATP but not glucose, while pH_G also greatly dropped (Fig. 2D and E). This suggests many compounds that impact ATP may also impact pH_G. Importantly, the impact on cellular ATP did not decrease cell viability within the timeframe the cells were incubated (Supplemental Fig. 3).

We next tested whether this method could identify specific types of glycolytic inhibitors, specifically inhibitors of glucose and pyruvate/proton transport. Phloretin has been shown to significantly decrease glucose import in BF *T. brucei* (Seyfang and Duszenko, 1991). As expected, 100 μM phloretin significantly decreased intracellular glucose and pH_G but not ATP (Supplemental Fig. 4). This provides evidence that compounds that perturb glucose levels likely target glucose transport.

Pyruvate export is important for maintaining physiological pH in BF *T. brucei* (Vanderheyden et al., 2000) and is a potential drug target (Sanchez, 2013). To test whether this method could identify inhibitors of pyruvate/proton export, we tested the effect of pyruvate (12.5 mM) on intracellular glucose, ATP, and pH_G in the presence of glucose. We expected that a high extracellular pyruvate concentration would inhibit normal pyruvate/proton efflux, resulting in a buildup of pyruvate and protons in the cell. Interestingly, pyruvate decreased pH_G more than the starved control but did not affect cytosolic glucose or ATP (Supplemental Fig. 5). This suggests that while pH_G, and likely cytosolic pH, were impacted by pyruvate, glycolysis remained unperturbed within this timeframe. This also provides evidence that compounds only decreasing pH_G likely target proton/pyruvate efflux.

While this multiplex screening method cannot conclusively identify compound target(s) or MOAs, we demonstrated this method can provide useful evidence suggesting possible targets(s)/MOA(s). This evidence can guide target-identification studies by providing evidence of glycolysis inhibition. In limited cases, this method can suggest specific targets/MOAs, specifically glucose import and pyruvate/proton export.

While gaining clues about a compound's MOA is very useful, the internal validation obtained from using multiple biosensors is also an important advantage of this method. Measuring multiple interrelated

Table 3
Individual and multiplexed measured Z-prime values in *T. brucei* BF for three biosensors.

Duplex	Biosensor	Analyte	Single Z'-Factor*	Multiplexed Z'-Factor*
YEMK and pHL	YEMK	ATP	0.97	0.93
	pHL	pH_G	0.79	0.68
FLIP700 and pHL	FLIP700	Glucose	0.83	0.95
	pHL	pH_G	0.79	0.77

* With slope correction.

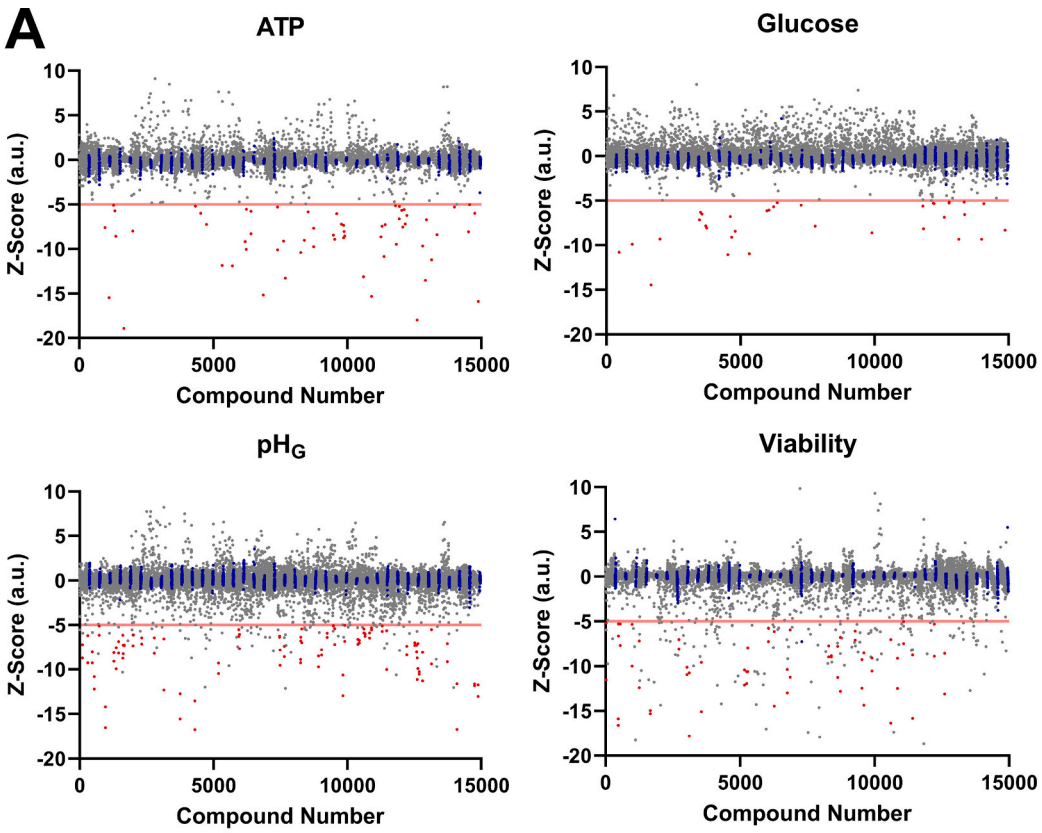

B

Sensor	Hit Rate (%)	Number of Unique Hits
ATP	0.4	61
Glucose	0.2	34
pH_G*	0.3	44
Viability*	0.2	32
Total	0.9	135

*Only repeat hits counted.

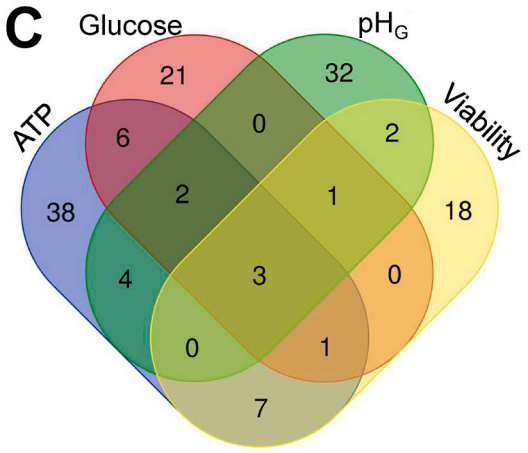

Fig. 3. Pilot screen of 14,976 compounds against ATP, glucose, glycosomal pH **(pH_G) sensors, and viability.** A) Results from the pilot screen included all compounds (gray), high controls with an equal DMSO concentration (0.1%) (blue), and hits (red). The red line on each graph indicates the −5 Z-score threshold used to distinguish hits. Compounds were measured twice for pH_G and Viability as part of the duplex screen; replicate hits are shown in red for these two analytes. Compounds were measured once for the Glucose and ATP biosensors, so all hits from these sensors are presented in red. B) Number of hits for each sensor and the hit rate for each sensor. C) Venn diagram of hits for each sensor, showing how information can be gained about a hit compound's possible target(s)/modes of action when using multiple sensors synergistically. Compounds that inhibit glucose transport are expected to perturb glucose, ATP, and pH_G. Inhibitors of glycolysis are expected to perturb ATP and pH_G but not glucose. Inhibitors of pyruvate/proton export are expected to perturb pH_G but not ATP or glucose. All hits for the ATP and glucose sensors are shown, while for the pH_G and viability sensors, only compounds that replicated activity are shown.(For interpretation of the references to colour in this figure legend, the reader is referred to the Web version of this article.)

analytes simultaneously provides internal validation of potential glycolytic inhibitors (Fig. 2B–D). This can increase confidence in hit compounds and decrease the impact of false positives in downstream testing.

3.4. Development of an HTS assay using flow cytometry and multiplexed biosensors

A multiplexed HTS assay using three different biosensor cell lines was used to screen for compounds that inhibit different parts of glycolysis. Supplemental Fig. 6 presents a diagram describing the sample preparation and data analysis for the HTS assay. Table 1 outlines the screening parameters according to the HTS Method Communication Guidelines (Inglese et al., 2007) with details provided in the Materials and Methods.

To make the assay as high throughput as possible while maintaining high data quality, various parameters and approaches were considered, including incubation conditions, robotic plate loading, incubation

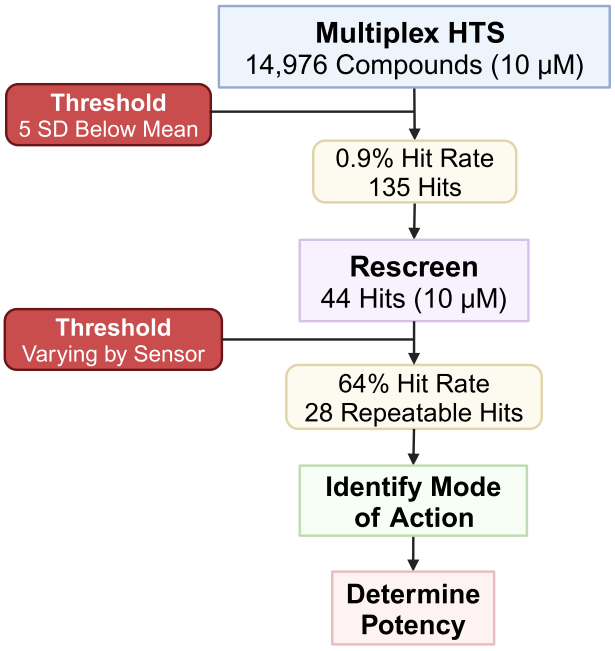

Fig. 4. Multiplex flow cytometry High-throughput screen workflow for discovering glycolytic inhibitors in *T. brucei*. A pilot screen of 14,976 compounds was screened at 10 μM against four sensors (ATP, glucose, glycosomal pH, and viability). We obtained an overall hit rate of 0.9% with 135 compounds that were hits in one or more sensors. We rescreened 44 of these hits to confirm activity; 64% (28 compounds) exhibited repeatable activity in one or more sensors. We identified helpful information about the putative mode of action for each repeatable hit based on what sensor(s) the hit impacted. Last, we determined the potency of the repeatable hits by measuring their EC_{50} values for each sensor they impacted. This diagram was created with BioRender.com.

temperature, number of cells collected, and flow rate.

Table 2 presents the protocol. For a more detailed protocol description, see the Methods section. To increase throughput to a reasonable level, multiple plates were prepared simultaneously and analyzed by flow cytometer at the fastest flow rate (1 mL/min). This did not significantly impact the measured Z′-factor (Zhang et al., 1999), supporting that this flow rate could be used without negatively impacting data quality (Supplemental Fig. 7, Supplemental Table 1). Through these optimization studies, we found that one mix per well was necessary to overcome cell settling, particularly when analyzing cold samples. Additionally, cells plated remained viable after a 1.5-h refrigeration incubation even after the 1.5-h room temperature incubation (~95% viable, Supplemental Fig. 8), with viability impacted only after a 3-h incubation (~92% viable). Based on these results, two 384-well plates were prepared at a time since each plate required ~1.5 h to run on the flow cytometer at the fastest flow rate. Together, these findings indicate this assay could be performed with moderately high throughput.

3.5. Pooling biosensors did not impact sensor response

To determine if multiplexing the three biosensors impacted data quality, we measured the Z′-factor value (Zhang et al., 1999) for each biosensor cell line both individually and multiplexed. As shown in Table 3, both multiplexed and individually ran biosensors gave acceptable Z′-factor values. Multiplexing only had a minor impact on sensor Z′-factor values. Individual and pooled Z′-factor figures are found in Supplemental Fig. 9 and Supplemental Fig. 10.

3.6. The pilot screen identified hits for each analyte

After optimizing the multiplex screening method, we performed a pilot screen on 14,976 compounds from the Life Chemicals Compound Library. To directly compare data across all plates, we chose to use the Z-Score method as this adequately allows samples to be compared across plates without the drawbacks inherent in using high and low controls (Brideau et al., 2003). We set the hit threshold at five SD below the mean of each plate, or a −5 Z-score, to achieve a hit rate between 0.1% and 1.0%, similar to most HTS assays (Shun et al., 2011). The number of hits and distribution of Z-scores for compounds and controls were different for each sensor (Fig. 3A). We observed that some high control wells with low numbers of total events or sensor events (less than 5000 events) sometimes resulted in Z-scores below the −5 threshold, so these were manually excluded due to poor data quality.

Interestingly, several compounds for each sensor had high Z-scores (5 SD above the mean). The flow cytometry data for many of these compounds showed the violet channel fluorescence of both biosensors was altered more than typically possible (Supplemental Figs. 11 and 12). Similar results have been observed when using fluorescent biosensors with the fluorescent compound doxycycline (Khader et al., 2014), suggesting these compounds were fluorescent. When we inspected samples with high Z-scores more closely, we observed that the less fluorescent subpopulation of each biosensor tended to increase the most in VL2-channel intensity, as expected for fluorescent compounds. Alternatively, some compounds with high Z-scores were due to the pHL population partially moving into the FLIP700 or YEMK gate. Based on this, we attributed these high Z-scores to compound fluorescence or movement of one biosensor into another's gate and did not pursue them further.

The ATP and pH_G sensors resulted in the most hits. In contrast, the glucose and viability sensors had the least (Fig. 3B). Many of the hits for the pH_G and viability sensors were found in replicate experiments, supporting the likelihood of their authenticity. The low hit rate for the glucose sensor may be because hexose transporters are the only known targets whose inhibition could decrease intracellular glucose (Fig. 2A). Many possible mechanisms could affect intracellular ATP, pH_G, or cell viability, supporting that these sensors would have higher hit rates. The low viability hit rate is likely because of the short incubation (1.5 h) compared to other viability screens (Siqueira-Neto et al., 2010; Bowling et al., 2012). The hit rates for all the sensors were below 1% but above 0.1% (Fig. 3B), a hit rate expected for most HTS assays (Shun et al., 2011). The hit rates for pH_G and viability were also decreased since non-repeatable hits were excluded when calculating these hit rates.

A Venn diagram was used to visualize the potential target(s)/MOAs of hits from the screen (Fig. 3C). Compounds perturbing glucose transport are expected to decrease glucose and possibly pH_G, ATP, and viability. Inhibitors of glycolysis and/or the associated glycerol-3-phosphate oxidase pathway were anticipated to decrease ATP, pH_G, and possibly viability while unaffecting glucose levels (Fig. 2A). Compounds that only impacted pH_G were hypothesized to target pH regulators in the glycosome, acidocalcisome, or plasma membrane as pH regulation from each of these cellular locations could influence pH_G (Vanderheyden et al., 2000; Lemercier et al., 2002; Lin et al., 2017). Compounds that only decreased viability likely target other cellular processes besides glycolysis.

While most hit compounds impacted only one sensor, several hits impacted multiple sensors (Fig. 3C). Surprisingly, most (~65%) of the compounds that perturbed glucose did not decrease ATP. This was unexpected as glucose is the primary source of ATP in BF *T. brucei*, particularly under these experimental conditions (Michels et al., 2021). A possible reason ATP was often unaffected by glucose inhibitors is intracellular glucose levels need to drop below a certain threshold before ATP levels decrease. This could be due to the ATP sensor's sensitivity range and/or the parasite's ability to maintain ATP under glucose-limiting conditions. To test this hypothesis, we incubated the

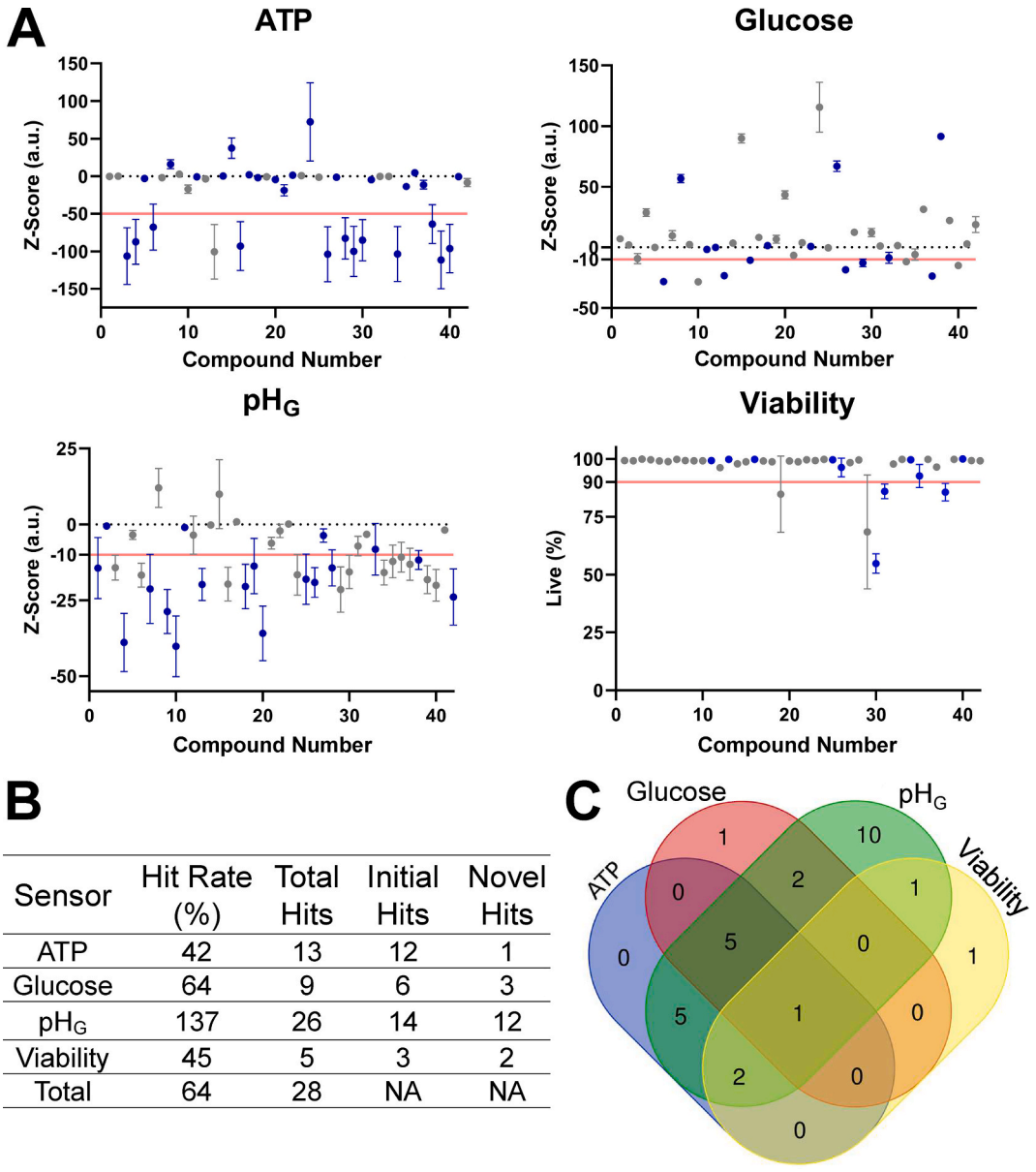

Sensor	Hit Rate (%)	Total Hits	Initial Hits	Novel Hits
ATP	42	13	12	1
Glucose	64	9	6	3
pH_G	137	26	14	12
Viability	45	5	3	2
Total	64	28	NA	NA

Fig. 5. A rescreen of 44 selected hit compounds demonstrated reproducible activity. A) Results from the rescreen for each sensor, including compounds that were hits for that sensor in the initial screen (blue) and compounds that were not (gray). The red line on each graph indicates the threshold used to distinguish hits. Two compounds were excluded as they showed evidence of autofluorescence. B) The percentage and number of compounds that were repeatable hits for each sensor in the rescreen compared to the initial screen. Some of these rescreen hits were hits in the initial screen (initial hits) and others were not (novel hits). C) Venn diagram of compounds that exhibited repeatable activity against one or more sensors. Comparing the compound's activity in these four sensors gives useful information about its potential target(s)/modes of action.(For interpretation of the references to colour in this figure legend, the reader is referred to the Web version of this article.)

two biosensor duplexes in serial dilutions of glucose and measured cytosolic glucose, ATP, and pH_G levels. ATP and pH_G began to drop at much lower concentrations of extracellular glucose than cytosolic glucose (Supplemental Fig. 13), supporting our hypothesis that intracellular glucose needs to drop close to the starved/low control before ATP and pH_G are impacted. This difference in the response for different sensors could also explain why most compounds impacting ATP or glucose did not affect pH_G in this initial screen. Alternatively, pH_G may not always correlate with ATP or glucose. This was observed when proton efflux was inhibited with high extracellular pyruvate while ATP and glucose levels remained unperturbed (Supplemental Fig. 5). Additionally, the pH_G and viability sensors experienced a more stringent selection before calculating hit rates and being included in the Venn diagram, as these two sensors had replicate measurements and non-repeating hits were excluded. This extra level of stringency could have resulted in fewer compounds being hits for ATP/glucose and pH_G.

3.7. Rescreening hits and determining their potency

After performing the pilot screen, we validated initial hits for each sensor (see the HTS workflow in Fig. 4). To validate initial hits, 44 compounds identified in the screen were reacquired from the University of Wisconsin-Madison Small Molecule Screening Facility and rescreened at 10 μM (Fig. 5). Most of the compounds we chose to rescreen were hits for more than one sensor. We excluded compounds that did not repeat activity against the pH_G sensor as each compound had two replicate measurements for this sensor. A few compounds that only impacted one sensor were also chosen for comparison. We used these criteria to confirm activity against multiple sensors and to determine if this screening method could identify compounds perturbing glycolysis.

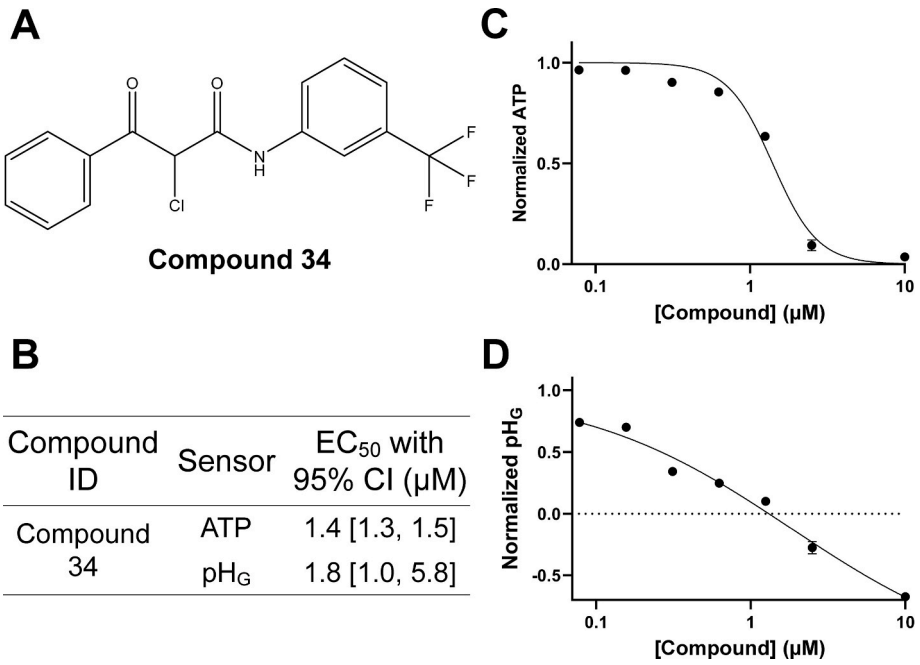

Fig. 6. A representative compound exhibited EC_{50} values below 10 μM for both ATP and glycosomal pH **(pH_G) sensors.** A) Structure of compound 34. B) Measured EC_{50} values for ATP and pH_G, with their associated 95% confidence intervals (CI). C) Impact of compound 34 on relative ATP. D) Impact of compound 34 on pH_G. The EC_{50} values were calculated by non-linear regression using the 4-parameter model shown in equation (6), where the Top and Bottom parameters were fixed to 1 and 0, respectively, for ATP, while only the TOP was fixed for pH_G.

Since we primarily rescreened compounds that perturbed more than one sensor, we expected most of these compounds to exhibit activity against multiple sensors. Overall, a high percentage of initial hits confirmed activity when rescreened (Fig. 5A and B) and most compounds did impact multiple sensors (Fig. 5C). We were surprised that some rescreened compounds exhibited significantly decreased Z-scores for sensor(s) that had not been perturbed in the initial screen (Fig. 5A and B). This was particularly true for pH_G. This was somewhat expected as the thresholds defining hits were different between the initial screen and the rescreen. This also suggests that rescreening hits in this assay can reveal activity against other sensors that may have been missed in the initial screen.

As seen in the initial screen, several compounds exhibited high Z-scores, particularly for the glucose sensor. We again attributed these high Z-scores to compound fluorescence and did not pursue those compounds. The Venn diagram in Fig. 5C shows that all compounds that impacted ATP also impacted pH_G, suggesting a strong biological relationship between these two analytes for the compounds tested. Most of the compounds that impacted glucose levels also impacted pH_G, again suggesting a relationship between these two analytes for these rescreened compounds. We also observed that most compounds impacting cell viability also impacted the other sensors, suggesting the toxicity of these compounds was due to their metabolic effect. Together, these results support that this screening method can identify compounds that perturb glycolysis, with each biosensor possessing a reasonable percentage of repeatable hits.

Next, we determined the potency of compounds that had repeatable activity by performing the multiplex screening assay on serial dilutions of each compound. Compound 34 (Fig. 6A) was representative of compounds that exhibited micromolar potency for both ATP and pH_G sensors. Compound 34 had similar EC_{50} values for both the ATP and pH_G sensors (Fig. 6B), suggesting these two analytes are associated with this compound. Compound 34 is likely an inhibiter of glycolysis as it impacts both ATP and pH_G in a dose-dependent manner (Fig. 6C and D). Interestingly, this compound caused pH_G to drop below the starved control (Fig. 6D), indicating this compound significantly acidified the glycosome, perhaps by inhibiting proton efflux from the cell/glycosome.

4. Conclusions

In this study, we developed a phenotypic HTS assay with some internal validation. Importantly, this HTS assay can provide clues about hit compounds' target(s) and MOA(s) by simultaneously measuring multiple glycolysis-relevant analytes. This fills an important gap present in most phenotypic screens: beginning the process of discovering the target(s) of hit compounds. While this method does not identify the precise molecular target(s) of hits, it does provide guidance by narrowing down the possible inhibitor targets. We accomplished this by multiplexing cell lines expressing FRET and GFP-based biosensors together and analyzing by flow cytometry, which builds upon recent related methods (Doucette et al., 2016). Sensors for glucose, ATP, and glycosomal pH have provided useful readouts of glycolysis in this organism, as BF *T. brucei* relies on glucose and glycolysis as its sole source of ATP in the mammalian bloodstream (Michels et al., 2021). Additionally, glycosomal pH is influenced by glucose in both BF and procyclic form *T. brucei* (Call et al., 2024), and ATP levels were shown to influence glycosomal pH in procyclic trypanosomes (Lin et al., 2017).

The results from this pilot screen show expected hit rates for each sensor and identify inhibitors with low micromolar potency. We are currently using this HTS assay to screen a large chemical library, and we will report on it soon.

The multiplexing strategy central to our HTS assay has several advantages compared to conventional screening methods, where only one analyte is measured. While multiplexing sensor cell lines together decreases flow cytometry run time and instrument cost, it also enables all sensor cell lines to experience the same treatment conditions. This increases the confidence in cross-correlations between different sensors during data analysis. As the analytes are interrelated, they can help validate hit compounds internally. A disadvantage of multiplexing is the increased assay and data analysis complexity. This increased complexity can somewhat decrease the assay throughput, but in our experience, this was minimal. One of the greatest challenges we found with multiplexing

was ensuring all sensor cell lines grew properly, as all cell lines were necessary to perform the assay.

Another disadvantage of screening with fluorescent biosensors is that compound fluorescence can negatively influence biosensor readings, preventing accurate measurement of the desired analyte(s) (Khader et al., 2014). We expect this problem will usually be small, as most libraries typically only have a small percentage of fluorescent compounds. If the library being screened has a high percentage of fluorescent compounds, a different method/strategy may be more appropriate.

While this screening assay can identify potential target(s) of hit compounds, further studies would be needed to determine their target(s) and MOA. These studies could include assays on specific suspected targets, such as in vitro enzymatic assays (Chambers et al., 2008; Joice et al., 2013), RNA interference (Han and Shi, 2018), and gene knockout/genetic mutation (Li et al., 1996; Morris et al., 2006). Unbiased approaches to identify drug target(s) include thermal proteome profiling (Mateus et al., 2017; Corpas-Lopez et al., 2019) and many others (Pasquer et al., 2020).

This multiplex screening method has the potential to identify novel glycolytic inhibitors that could be used as chemical probes to study metabolism in *T. brucei* and related parasites such as T. cruzi and Leishmania spp. We expect that chemical probes discovered from this screening method will improve our understanding of kinetoplastid metabolism and biology, opening new ways to treat these diseases and combat drug resistance.

CRediT authorship contribution statement

Daniel H. Call: Writing – review & editing, Writing – original draft, Visualization, Validation, Project administration, Methodology, Investigation, Formal analysis, Data curation. **John Asafo Adjei:** Writing – original draft, Visualization, Investigation, Formal analysis. **Ryan Pilgrim:** Writing – original draft, Visualization, Validation, Methodology, Investigation, Formal analysis, Data curation. **James W. Jeong:** Writing – original draft, Visualization, Investigation. **E. Vance Willis:** Methodology, Investigation. **Ronald A. Zegarra:** Methodology, Investigation, Parker Evans, Resources, Investigation. **Nicholas L. Tapia:** Formal analysis, Investigation, Methodology. **Madalyn Osterhaus:** Methodology, Investigation. **Jacob A. Vance:** Methodology, Investigation. **Charles M. Voyton:** Writing – review & editing, Methodology. **James A. Call:** Writing – review & editing, Writing – original draft, Software. **Sabrina S. Pizarro:** Resources. **James C. Morris:** Writing – review & editing, Resources, Funding acquisition. **Kenneth A. Christensen:** Writing – review & editing, Supervision, Resources, Methodology, Funding acquisition, Conceptualization.

Declaration of generative AI and AI-assisted technologies in the writing process

During the preparation of this work, the author(s) used Grammarly to improve text grammar and readability. After using this tool/service, the author(s) reviewed and edited the content as needed and take(s) full responsibility for the publication's content.

Declaration of competing interest

All authors declare that they have no conflicts of interest.

Acknowledgments

We want to thank Dr. Karl Werbovetz of The Ohio State University College of Pharmacy for his input on the manuscript. We also thank Dr. Jennifer Golden of the University of Wisconsin for her input on the hit compounds. This work was supported by the National Institutes of Health [grant number R01AI156382, 2020 and 2024] and Brigham Young University, which provided funding for RP, JWJ, EVW, RAZ, MO, and JAV.

Appendix A. Supplementary data

Supplementary data to this article can be found online at https://doi.org/10.1016/j.ijpddr.2024.100557.

References

Bakker, B.M., Michels, P.A.M., Opperdoes, F.R., Westerhoff, H.V., 1999. What controls glycolysis in bloodstream form trypanosoma brucei? J. Biol. Chem. 274, 14551–14559. https://doi.org/10.1074/jbc.274.21.14551.

Barban, S., Schulze, H.O., 1961. The effects of 2-deoxyglucose on the growth and metabolism of cultured human cells. J. Biol. Chem. 236, 1887–1890. https://doi.org/10.1016/S0021-9258(18)64100-6.

Bermejo, C., Haerizadeh, F., Takanaga, H., Chermak, D., Frommer, W.B., 2010. Dynamic analysis of cytosolic glucose and ATP levels in yeast using optical sensors. Biochem. J. 432, 399–406. https://doi.org/10.1042/BJ20100946.

Bowling, T., Mercer, L., Don, R., Jacobs, R., Nare, B., 2012. Application of a resazurin-based high-throughput screening assay for the identification and progression of new treatments for human African trypanosomiasis. Int J Parasitol Drugs Drug Resist 2, 262–270. https://doi.org/10.1016/j.ijpddr.2012.02.002.

Brideau, C., Gunter, B., Pikounis, B., Liaw, A., 2003. Improved statistical methods for hit selection in high-throughput screening. J. Biomol. Screen 8, 634–647. https://doi.org/10.1177/1087057103258285.

Call, D., Pizarro, S.S., Tovey, E., Knight, E., Baumgardner, C., Christensen, K.A., Morris, J.C., 2024. Measuring dynamic glycosomal pH changes in living trypanosoma brucei. JoVE 66279. https://doi.org/10.3791/66279.

Chambers, J.W., Fowler, M.L., Morris, M.T., Morris, J.C., 2008. The anti-trypanosomal agent lonidamine inhibits Trypanosoma brucei hexokinase 1. Mol. Biochem. Parasitol. 158, 202–207. https://doi.org/10.1016/j.molbiopara.2007.12.013.

Chaudhuri, M., Ott, R.D., Hill, G.C., 2006. Trypanosome alternative oxidase: from molecule to function. Trends Parasitol. 22, 484–491. https://doi.org/10.1016/j.pt.2006.08.007.

Clarkson, A.B., Brohn, F.H., 1976. Trypanosomiasis: an approach to chemotherapy by the inhibition of carbohydrate catabolism. Science 194, 204–206. https://doi.org/10.1126/science.986688.

Clarkson, A.B., Grady, R.W., Grossman, S.A., McCallum, R.J., Brohn, F.H., 1981. Trypanosoma brucei brucei: a systematic screening for alternatives to the salicylhydroxamic acid-glycerol combination. Mol. Biochem. Parasitol. 3, 271–291. https://doi.org/10.1016/0166-6851(81)90002-5.

Coley, A.F., Dodson, H.C., Morris, M.T., Morris, J.C., 2011. Glycolysis in the African trypanosome: targeting enzymes and their subcellular compartments for therapeutic development. Mol Biol Int 2011, 123702. https://doi.org/10.4061/2011/123702.

Corpas-Lopez, V., Moniz, S., Thomas, M., Wall, R.J., Torrie, L.S., Zander-Dinse, D., Tinti, M., Brand, S., Stojanovski, L., Manthri, S., Hallyburton, I., Zuccotto, F., Wyatt, P.G., De Rycker, M., Horn, D., Ferguson, M.A.J., Clos, J., Read, K.D., Fairlamb, A.H., Gilbert, I.H., Wyllie, S., 2019. Pharmacological validation of N-myristoyltransferase as a drug target in Leishmania donovani. ACS Infect. Dis. 5, 111–122. https://doi.org/10.1021/acsinfecdis.8b00226.

Ding, M., Clark, R., Bardelle, C., Backmark, A., Norris, T., Williams, W., Wigglesworth, M., Howes, R., 2018. Application of high-throughput flow cytometry in early drug discovery: an AstraZeneca perspective. SLAS DISCOVERY: Advancing the Science of Drug Discovery 23, 719–731. https://doi.org/10.1177/2472555218775074.

Dodson, H.C., Morris, M.T., Morris, J.C., 2011. Glycerol 3-phosphate alters trypanosoma brucei hexokinase activity in response to environmental change. J. Biol. Chem. 286, 33150–33157. https://doi.org/10.1074/jbc.M111.235705.

Doucette, J., Zhao, Z., Geyer, R.J., Barra, M.M., Balunas, M.J., Zweifach, A., 2016. Flow cytometry enables multiplexed measurements of genetically encoded intramolecular FRET sensors suitable for screening. J. Biomol. Screen 21, 535–547. https://doi.org/10.1177/1087057116634007.

Ebiloma, G.U., Balogun, E.O., Cueto-Díaz, E.J., Koning, H.P.d., Dardonville, C., 2019. Alternative oxidase inhibitors: mitochondrion-targeting as a strategy for new drugs against pathogenic parasites and fungi. Med. Res. Rev. 39, 1553–1602. https://doi.org/10.1002/med.21560.

Eshetu, E., Begejo, B., 2015. The current situation and diagnostic approach of nagana in Africa: a review. J. Nat. Sci. Res. 5, 117–124. https://www.cabidigitallibrary.org/doi/full/10.5555/20153366849.

Fehr, M., Lalonde, S., Lager, I., Wolff, M.W., Frommer, W.B., 2003. In vivo imaging of the dynamics of glucose uptake in the cytosol of COS-7 cells by fluorescent nanosensors. J. Biol. Chem. 278, 19127–19133. https://doi.org/10.1074/jbc.M301333200.

Gaspar, L., Moraes, C.B., Freitas-Junior, L.H., Ferrari, S., Costantino, L., Costi, M.P., Coron, R.P., Smith, T.K., Siqueira-Neto, J.L., McKerrow, J.H., Cordeiro-da-Silva, A., 2015. Current and future chemotherapy for Chagas disease. Curr. Med. Chem. 22, 4293–4312. https://doi.org/10.2174/0929867322666151015120804.

Gilbert, I.H., 2013. Drug discovery for neglected diseases: molecular target-based and phenotypic approaches. J. Med. Chem. 56, 7719–7726. https://doi.org/10.1021/jm400362b.

Ginger, M.L., Ngazoa, E.S., Pereira, C.A., Pullen, T.J., Kabiri, M., Becker, K., Gull, K., Steverding, D., 2005. Intracellular positioning of isoforms explains an unusually large adenylate kinase gene family in the parasite trypanosoma brucei. J. Biol. Chem. 280, 11781–11789. https://doi.org/10.1074/jbc.M413821200.

Gruenberg, J., Sharma, P.R., Deshusses, J., 1978. d-Glucose Transport in Trypanosoma brucei. Eur. J. Biochem. 89, 461–469. https://doi.org/10.1111/j.1432-1033.1978.tb12549.x.

Gualdrón-López, M., Brennand, A., Avilán, L., Michels, P.a.M., 2013. Translocation of solutes and proteins across the glycosomal membrane of trypanosomes; possibilities and limitations for targeting with trypanocidal drugs. Parasitology 140, 1–20. https://doi.org/10.1017/S0031182012001278.

Gualdron-López, M., Vapola, M.H., Miinalainen, I.J., Hiltunen, J.K., Michels, P.A.M., Antonenkov, V.D., 2012. Channel-forming activities in the glycosomal fraction from the bloodstream form of trypanosoma brucei. PLoS One 7, e34530. https://doi.org/10.1371/journal.pone.0034530.

Han, Z., Shi, L., 2018. Long non-coding RNA LUCAT1 modulates methotrexate resistance in osteosarcoma via miR-200c/ABCB1 axis. Biochem. Biophys. Res. Commun. 495, 947–953. https://doi.org/10.1016/j.bbrc.2017.11.121.

Hefnawy, A., Berg, M., Dujardin, J.-C., De Muylder, G., 2017. Exploiting knowledge on Leishmania drug resistance to support the quest for new drugs. Trends Parasitol. 33, 162–174. https://doi.org/10.1016/j.pt.2016.11.003.

Helfert, S., Estévez, A.M., Bakker, B., Michels, P., Clayton, C., 2001. Roles of triosephosphate isomerase and aerobic metabolism in Trypanosoma brucei. Biochem. J. 357, 117–125. https://doi.org/10.1042/0264-6021:3570117.

Höög, J.L., Gluenz, E., Vaughan, S., Gull, K., 2010. Ultrastructural investigation methods for trypanosoma brucei. Methods Cell Biol. 96, 175–196. https://doi.org/10.1016/S0091-679X(10)96008-1.

Igoillo-Esteve, M., Mazet, M., Deumer, G., Wallemacq, P., Michels, P.A.M., 2011. Glycosomal ABC transporters of Trypanosoma brucei: characterisation of their expression, topology and substrate specificity. Int. J. Parasitol. 41, 429–438. https://doi.org/10.1016/j.ijpara.2010.11.002.

Imamura, H., Nhat, K.P.H., Togawa, H., Saito, K., Iino, R., Kato-Yamada, Y., Nagai, T., Noji, H., 2009. Visualization of ATP levels inside single living cells with fluorescence resonance energy transfer-based genetically encoded indicators. Proc. Natl. Acad. Sci. USA 106, 15651–15656. https://doi.org/10.1073/pnas.0904764106.

Inglese, J., Shamu, C.E., Guy, R.K., 2007. Reporting data from high-throughput screening of small-molecule libraries. Nat. Chem. Biol. 3, 438–441. https://doi.org/10.1038/nchembio0807-438.

Janzen, William P., 2014. Screening technologies for small molecule discovery: the state of the art. Chem. Biol. 21, 1162–1170. https://doi.org/10.1016/j.chembiol.2014.07.015.

Joice, A.C., Harris, M.T., Kahney, E.W., Dodson, H.C., Maselli, A.G., Whitehead, D.C., Morris, J.C., 2013. Exploring the mode of action of ebselen in Trypanosoma brucei hexokinase inhibition. Int. J. Parasitol.: Drugs Drug Resist. 3, 154–160. https://doi.org/10.1016/j.ijpddr.2013.08.002.

Katsuno, K., Burrows, J.N., Duncan, K., van Huijsduijnen, R.H., Kaneko, T., Kita, K., Mowbray, C.E., Schmatz, D., Warner, P., Slingsby, B.T., 2015. Hit and lead criteria in drug discovery for infectious diseases of the developing world. Nat. Rev. Drug Discov. 14, 751–758. https://doi.org/10.1038/nrd4683.

Khader, H., Solodushko, V., Al-Mehdi, A.B., Audia, J., Fouty, B., 2014. Overlap of doxycycline fluorescence with that of the redox-sensitive intracellular reporter roGFP. J. Fluoresc. 24, 305–311. https://doi.org/10.1007/s10895-013-1331-6.

Kovářová, J., Nagar, R., Faria, J., Ferguson, M.A.J., Barrett, M.P., Horn, D., 2018. Gluconeogenesis using glycerol as a substrate in bloodstream-form Trypanosoma brucei. PLoS Pathog. 14, e1007475 https://doi.org/10.1371/journal.ppat.1007475.

Krutzik, P.O., Nolan, G.P., 2006. Fluorescent cell barcoding in flow cytometry allows high-throughput drug screening and signaling profiling. Nat. Methods 3, 361. https://doi.org/10.1038/nmeth872.

Laussel, C., Léon, S., 2020. Cellular toxicity of the metabolic inhibitor 2-deoxyglucose and associated resistance mechanisms. Biochem. Pharmacol. 182, 114213 https://doi.org/10.1016/j.bcp.2020.114213.

Lemercier, G., Dutoya, S., Luo, S., Ruiz, F.A., Rodrigues, C.O., Baltz, T., Docampo, R., Bakalara, N., 2002. A vacuolar-type H+-Pyrophosphatase governs maintenance of functional acidocalcisomes and growth of the insect and mammalian forms of trypanosoma brucei. J. Biol. Chem. 277, 37369–37376. https://doi.org/10.1074/jbc.M204744200.

Li, F., Hua, S.b., Wang, C.C., Gottesdiener, K.M., 1996. Procyclic Trypanosoma brucei cell lines deficient in ornithine decarboxylase activity. Mol. Biochem. Parasitol. 78, 227–236. https://doi.org/10.1016/S0166-6851(96)02630-8.

Lin, S., Voyton, C., Morris, M.T., Ackroyd, P.C., Morris, J.C., Christensen, K.A., 2017. pH regulation in glycosomes of procyclic form Trypanosoma brucei. J. Biol. Chem. 292, 7795–7805. https://doi.org/10.1074/jbc.M117.784173.

Mahon, M.J., 2011. pHluorin2: an enhanced, ratiometric, pH-sensitive green florescent protein. Adv. Biosci. Biotechnol. 2, 132–137. https://doi.org/10.4236/abb.2011.23021.

Mateus, A., Määttä, T.A., Savitski, M.M., 2017. Thermal proteome profiling: unbiased assessment of protein state through heat-induced stability changes. Proteome Sci. 15 https://doi.org/10.1186/s12953-017-0122-4.

McNae, I.W., Kinkead, J., Malik, D., Yen, L.-H., Walker, M.K., Swain, C., Webster, S.P., Gray, N., Fernandes, P.M., Myburgh, E., Blackburn, E.A., Ritchie, R., Austin, C., Wear, M.A., Highton, A.J., Keats, A.J., Vong, A., Dornan, J., Mottram, J.C., Michels, P.A.M., Pettit, S., Walkinshaw, M.D., 2021. Fast acting allosteric phosphofructokinase inhibitors block trypanosome glycolysis and cure acute African trypanosomiasis in mice. Nat. Commun. 12, 1052. https://doi.org/10.1038/s41467-021-21273-6.

Mesu, V.K.B.K., Kalonji, W.M., Bardonneau, C., Mordt, O.V., Blesson, S., Simon, F., Delhomme, S., Bernhard, S., Kuziena, W., Lubaki, J.-P.F., Vuvu, S.L., Ngima, P.N., Mbembo, H.M., Ilunga, M., Bonama, A.K., Heradi, J.A., Solomo, J.L.L., Mandula, G., Badibabi, L.K., Dama, F.R., Lukula, P.K., Tete, D.N., Lumbala, C., Scherrer, B., Strub-Wourgaft, N., Tarral, A., 2018. Oral fexinidazole for late-stage African Trypanosoma brucei gambiense trypanosomiasis: a pivotal multicentre, randomised, non-inferiority trial. Lancet 391, 144–154. https://doi.org/10.1016/S0140-6736(17)32758-7.

Michels, P.A.M., Villafraz, O., Pineda, E., Alencar, M.B., Cáceres, A.J., Silber, A.M., Bringaud, F., 2021. Carbohydrate metabolism in trypanosomatids: new insights revealing novel complexity, diversity and species-unique features. Exp. Parasitol., 108102 https://doi.org/10.1016/j.exppara.2021.108102.

Molyneux, D.H., Savioli, L., Engels, D., 2017. Neglected tropical diseases: progress towards addressing the chronic pandemic. Lancet 389, 312–325. https://doi.org/10.1016/S0140-6736(16)30171-4.

Morris, M.T., DeBruin, C., Yang, Z., Chambers, J.W., Smith, K.S., Morris, J.C., 2006. Activity of a second trypanosoma brucei hexokinase is controlled by an 18-amino-acid C-terminal tail. Eukaryot. Cell 5, 2014–2023. https://doi.org/10.1128/EC.00146-06.

Nwagwu, M., Opperdoes, F., 1982. Regulation of glycolysis in Trypanosoma brucei: hexokinase and phosphofructokinase activity. Acta Trop. 39, 61–72. https://pubmed.ncbi.nlm.nih.gov/6122364/.

Opperdoes, F.R., Borst, P., 1977. Localization of nine glycolytic enzymes in a microbody-like organelle in Trypanosoma brucei: the glycosome. FEBS (Fed. Eur. Biochem. Soc.) Lett. 80, 360–364. https://doi.org/10.1016/0014-5793(77)80476-6.

Pasquer, Q.T.L., Tsakoumagkos, I.A., Hoogendoorn, S., 2020. From phenotypic hit to chemical probe: chemical biology approaches to elucidate small molecule action in complex biological systems. Molecules 25. https://doi.org/10.3390/molecules25235702.

Ponte-Sucre, A., Gamarro, F., Dujardin, J.-C., Barrett, M.P., López-Vélez, R., García-Hernández, R., Pountain, A.W., Mwenechanya, R., Papadopoulou, B., 2017. Drug resistance and treatment failure in leishmaniasis: a 21st century challenge. PLoS Neglected Trop. Dis. 11, e0006052 https://doi.org/10.1371/journal.pntd.0006052.

Qiu, Y., Milanes, J.E., Jones, J.A., Noorai, R.E., Shankar, V., Morris, J.C., 2018. Glucose signaling is important for nutrient adaptation during differentiation of pleomorphic african trypanosomes. mSphere 3, e00366. https://doi.org/10.1128/mSphere.00366-18, 00318.

Roster, C.P., LaVigne, D., Milanes, J.E., Knight, E., Anderson, H.D., Pizarro, S., Harding, E.M., Morris, M.T., Yan, V.C., Pham, C.-D., Muller, F., Kwain, S., Rees, K.C., Dominy, B., Whitehead, D.C., Uddin, M.N., Millward, S.W., Morris, J.C., 2023. Enolase inhibitors as early lead therapeutics against trypanosoma brucei. Pathogens 12, 1290. https://doi.org/10.3390/pathogens12111290.

Russo, I., Oksman, A., Vaupel, B., Goldberg, D.E., 2009. A calpain unique to alveolates is essential in Plasmodium falciparum and its knockdown reveals an involvement in pre-S-phase development. Proceedings of the National Academy of Sciences of the United States of America 106, 1554–1559. https://doi.org/10.1073/pnas.0806926106.

Sanchez, M.A., 2013. Molecular identification and characterization of an essential pyruvate transporter from trypanosoma brucei. J. Biol. Chem. 288, 14428–14437. https://doi.org/10.1074/jbc.M113.473157.

Seyfang, A., Duszenko, M., 1991. Specificity of glucose transport in Trypanosoma brucei. Eur. J. Biochem. 202, 191–196. https://doi.org/10.1111/j.1432-1033.1991.tb16362.x.

Sharlow, E.R., Lyda, T.A., Dodson, H.C., Mustata, G., Morris, M.T., Leimgruber, S.S., Lee, K.-H., Kashiwada, Y., Close, D., Lazo, J.S., Morris, J.C., 2010. A target-based high throughput screen yields trypanosoma brucei hexokinase small molecule inhibitors with antiparasitic activity. PLoS Neglected Trop. Dis. 4, e659. https://doi.org/10.1371/journal.pntd.0000659.

Shun, T.Y., Lazo, J.S., Sharlow, E.R., Johnston, P.A., 2011. Identifying actives from HTS data sets: practical approaches for the selection of an appropriate HTS data-processing method and quality control review. J. Biomol. Screen 16, 1–14. https://doi.org/10.1177/1087057110389039.

Siqueira-Neto, J.L., Song, O.-R., Oh, H., Sohn, J.-H., Yang, G., Nam, J., Jang, J., Cechetto, J., Lee, C.B., Moon, S., Genovesio, A., Chatelain, E., Christophe, T., Freitas-Junior, L.H., 2010. Antileishmanial high-throughput drug screening reveals drug candidates with new scaffolds. PLoS Neglected Trop. Dis. 4, e675 https://doi.org/10.1371/journal.pntd.0000675.

Spurgeon, B.E.J., Naseem, K.M., 2020. Phosphoflow cytometry and barcoding in blood platelets: technical and analytical considerations. Cytometry B Clin. Cytometry 98, 123–130. https://doi.org/10.1002/cyto.b.21851.

St Onge, R., Schlecht, U., Scharfe, C., Evangelista, M., 2012. Forward chemical genetics in yeast for discovery of chemical probes targeting metabolism. Molecules 17, 13098–13115. https://doi.org/10.3390/molecules171113098.

Swinney, D.C., 2013. Phenotypic vs. Target-based drug discovery for first-in-class medicines. Clinical Pharmacology & Therapeutics 93, 299–301. https://doi.org/10.1038/clpt.2012.236.

Szöőr, B., Ruberto, I., Burchmore, R., Matthews, K.R., 2010. A novel phosphatase cascade regulates differentiation in Trypanosoma brucei via a glycosomal signaling pathway. Genes Dev. 24, 1306–1316. https://doi.org/10.1101/gad.570310.

Tetaud, E., Giroud, C., Prescott, A.R., Parkin, D.W., Baltz, D., Biteau, N., Baltz, T., Fairlamb, A.H., 2001. Molecular characterisation of mitochondrial and cytosolic trypanothione-dependent tryparedoxin peroxidases in Trypanosoma brucei. Mol. Biochem. Parasitol. 116, 171–183. https://doi.org/10.1016/S0166-6851(01)00320-6.

Uzcategui, N.L., Szallies, A., Pavlovic-Djuranovic, S., Palmada, M., Figarella, K., Boehmer, C., Lang, F., Beitz, E., Duszenko, M., 2004. Cloning, heterologous expression, and characterization of three aquaglyceroporins from trypanosoma brucei. J. Biol. Chem. 279, 42669–42676. https://doi.org/10.1074/jbc.M404518200.

Vanderheyden, N., Wong, J., Docampo, R., 2000. A pyruvate-proton symport and an H+-ATPase regulate the intracellular pH of Trypanosoma brucei at different stages of its life cycle. Biochem. J. 346, 53–62.

Voyton, C.M., Morris, M.T., Ackroyd, P.C., Morris, J.C., Christensen, K.A., 2018a. FRET flow cytometry-based high throughput screening assay to identify disrupters of glucose levels in trypanosoma brucei. ACS Infect. Dis. 4, 1058–1066. https://doi.org/10.1021/acsinfecdis.8b00058.

Voyton, C.M., Qiu, Y., Morris, M.T., Ackroyd, P.C., Suryadi, J., Crowe, L., Morris, J.C., Christensen, K.A., 2018b. A FRET flow cytometry method for monitoring cytosolic and glycosomal glucose in living kinetoplastid parasites. PLoS Neglected Trop. Dis. 12, e0006523 https://doi.org/10.1371/journal.pntd.0006523.

Wang, Z., Morris, J.C., Drew, M.E., Englund, P.T., 2000. Inhibition of trypanosoma brucei gene expression by RNA interference using an integratable vector with opposing T7 promoters. J. Biol. Chem. 275, 40174–40179. https://doi.org/10.1074/jbc.M008405200.

Wick, A.N., Drury, D.R., Nakada, H.I., Wolfe, J.B., Britton, B., Grabowski, R., 1957. Localization of the primary metabolic block produced by 2-DEOXYGLUCOSE. J. Biol. Chem. 224, 963–969. https://doi.org/10.1016/S0021-9258(18)64988-9.

Wiemer, E.A., Michels, P.A., Opperdoes, F.R., 1995. The inhibition of pyruvate transport across the plasma membrane of the bloodstream form of Trypanosoma brucei and its metabolic implications. Biochem. J. 312, 479–484. https://doi.org/10.1042/bj3120479.

World Health Organization, 2015. Investing to overcome the global impact of neglected tropical diseases: third WHO report on neglected tropical diseases 2015, 211. https://www.who.int/publications/i/item/9789241564861.

World Health Organization, Department of Control of Neglected Tropical Diseases, 2017. Integrating neglected tropical diseases into global health and development. fourth WHO report on neglected tropical diseases 278. https://www.who.int/publications/i/item/9789241565448.

Wu, W., Wang, X., Shen, M., Li, L., Yin, Y., Shen, L., Wang, W., Cui, D., Ni, J., Chen, X., Li, W., 2019. AIEgens barcodes combined with AIEgens nanobeads for high-sensitivity multiplexed detection. Theranostics 9, 7210–7221. https://doi.org/10.7150/thno.36525.

Zhang, J.-H., Chung, T.D.Y., Oldenburg, K.R., 1999. A simple statistical parameter for use in evaluation and validation of high throughput screening assays. J. Biomol. Screen 4, 67–73. https://doi.org/10.1177/108705719900400206.